Initial Astronomical Results with a New 5 - 14 μm Si:Ga 58 X 62 DRO Array Camera

Dan Gezari, Walter Folz, and Larry Woods

NASA/Goddard Space Flight Center
Infrared Astrophysics Branch, Code 685, Greenbelt, MD 20771

A new array camera system has been developed using a 58 x 62 pixel Si:Ga (gallium doped silicon) DRO (direct readout) photoconductor array detector manufactured by Hughes/ Santa Barbara Research Center (SBRC). The camera system is a broad band photometer designed for 5 - 14 μm imaging with large ground-based optical telescopes. In a typical application a 10 μm photon flux of about 10^9 photons $sec^{-1}m^{-2}\mu m^{-1}$ $arcsec^{-2}$ is incident in the telescope focal plane, while the detector well capacity of these arrays is 10^5-10^6 electrons. However, when the real efficiencies and operating conditions are accounted for, the 2-channel 3596 pixel array operates with about 1/2 full wells at 10 μm and 10% bandwidth with high duty cycle and no real experimental compromises.

CAMERA SYSTEM AND PERFORMANCE:

The 58 x 62 Si:Ga DRO Array:

The SBRC DRO array is a hybrid device, assembled from an optimized Si:Ga detector wafer bump-bonded to a CRC-228 multiplexer, with stable electronic and photometric characteristics (c. f. Hoffman 1987). The same 58 x 62 CRC-228 multiplexer is used in the SBRC 1 - 5 μm photovoltaic InSb (indium antimonide) arrays, and has been characterized for astronomical applications by several groups (McLean et al. 1986; Fowler et al. 1987a, 1987b; Ninkov, Forrest and Pipher 1987; McCaughrean 1988). The 15 - 30 μm Si:Sb (antimony doped silicon) version in this family of SBRC arrays has been described by McKelvey et al. (1987).

This Si:Ga DRO array (operating at 12 Kelvin) has a detector capacitance = 0.07 pF with a net bias of 10 volts, based on a measured full well capacity = 7 x 10^5 electrons, an ηG_{pc} product ~ 0.2, read noise < 200 electrons/read, dark current < 630 electrons/sec (light leak limited), gain variation among pixels ~ 15% correctable to < 0.1% by flat fielding, active pixels > 99%, and crosstalk < 5%.

Camera Electronics and Data System:

The camera electronics system (Figure 1) is divided into three sub-systems: 1) analog front-end electronics (Folz 1988), including low noise 2-channel preamp modules, high-speed A/D converters, regulated low-noise bias power supplies, timing generator, timing signal buffer, and detector temperature monitor/regulator, 2) digital data acquisition section based on a Q-bus Mercury ZIP 3216 arithmetic array processor and 3) DEC LSI 11/73 host computer for camera control and data analysis. A detailed description of the camera system analog and digital electronics is given by Gezari et al. (1988).

In low background applications correlated triple sampling is used to achieve detector-limited noise performance (<100 electrons/read) by suppressing 1/f noise, kTC reset

noise, and similar small effects. However, at high-backgrounds the measured noise is limited by fluctuations in the thermal photon background at the ~1000 electron level, and detector noise sources are negligible. For applications requiring a faster frame rate, carefully calibrated single sampling is used to operate at 60 Hz without sacrificing noise performance. The full 16 bit resolution of the A/D converters is not required for high-background applications, but would be used for low- background experiments with large dynamic range.

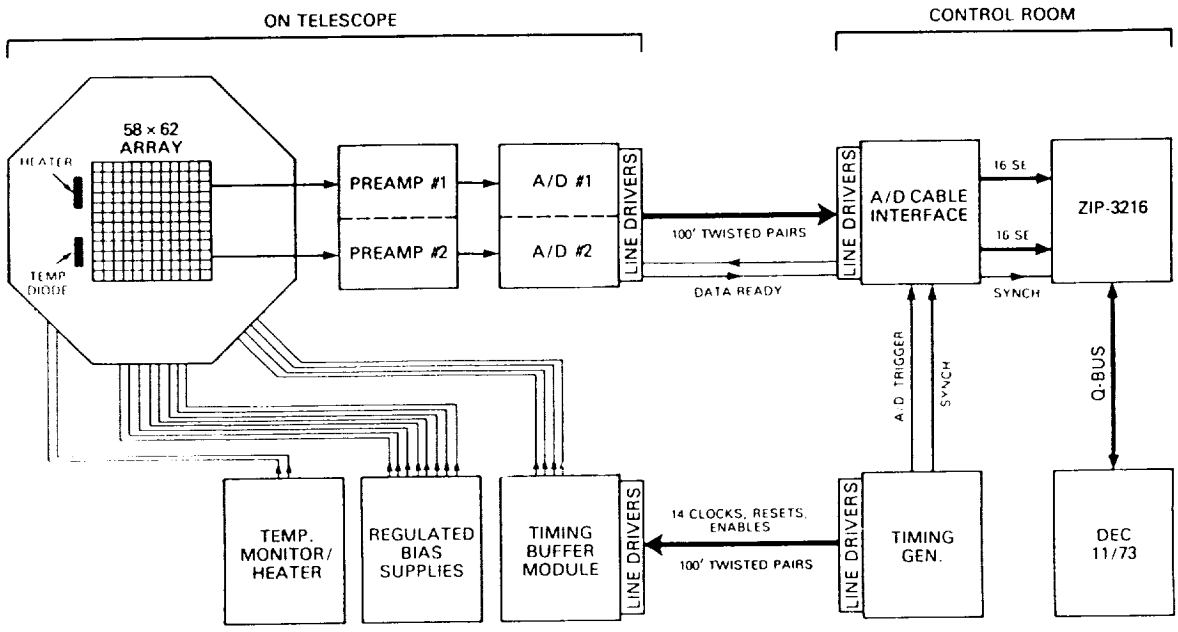

Figure 1: The electronic design of the 58 x 62 Si:Ga DRO camera system.

Cryogenic Optical System Design:

The array camera uses an off-axis reflective optical design (Gezari 1988a) which produces diffraction-limited images with good background radiation suppression. A single off-axis 3.0-inch focal length parabolic mirror, 0.7-inch square, is the only focusing element. The telescope optical axis is located 0.75 inches off the axis of the parabola (figure 2). The parabola re-images the telescope focal plane (located 1 inch outside the dewar) on the array with a de-magnification of 2:1, resulting in an array plate scale on the f/35 3-meter IRTF telescope of 0.26 arcsec per pixel. This permits for rigorous sampling of diffraction-limited image information (two pixels per airy FWHM at 8 μm) and gives a field-of-view on the IRTF of 14.9 x 16.3 ($\pm$ 0.1) arcsec. The parabola also makes an image of the f/35 secondary mirror at a 0.09 inch diameter cold aperture stop on the parabola axis. The cold stop defines the spectral bandwidth of the circular variable filter (CVF) to be 0.4 μm at 10 microns. Another filter wheel contains set of 10% bandwidth OCLI fixed interference filters at 7.9, 8.7, 9.8, 10.3, 11.6 and 12.4 μm. The net optical efficiency (telescope, photometer dichroic and dewar optics) is about 10% (dominated by ~ 50% transmission CVF filter). The camera is diffraction-limited at wavelengths $\lambda > 5$ μm and typically produces seeing-limited 1.0 $\pm$ 0.1 arcsecond stellar images in long integrations

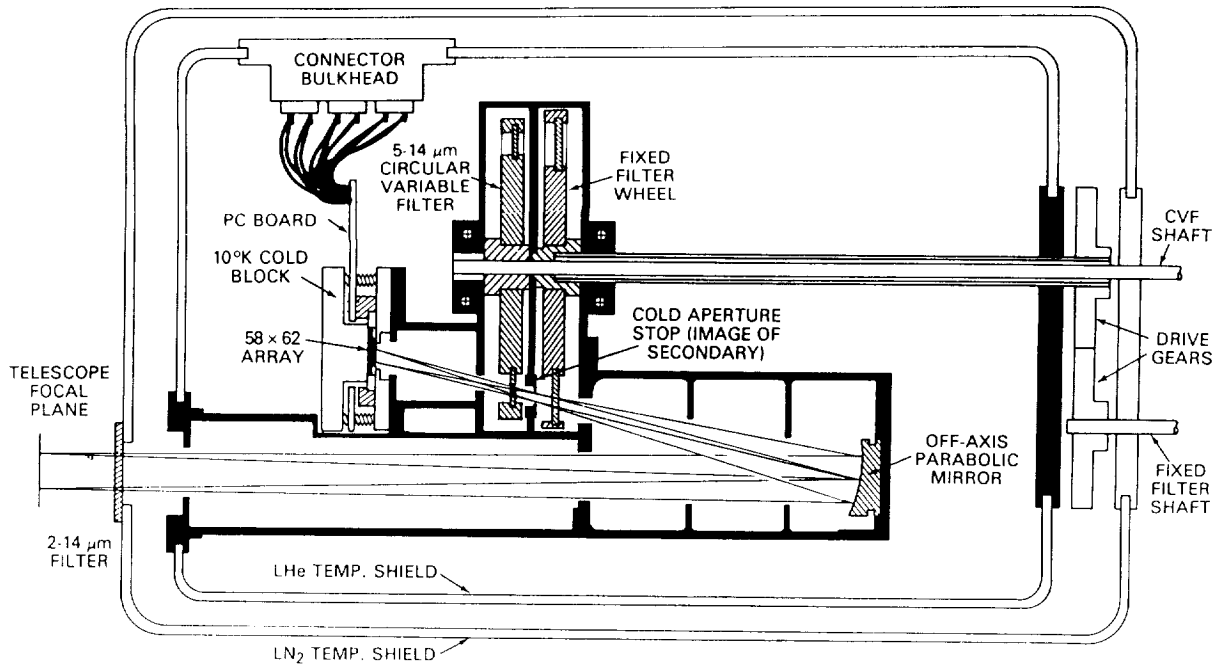

Figure 2: Optical design and mechanical layout of the cryogenic dewar optical bench, showing the arrangement of the off-axis parabola, cold aperture stop at the image of the telescope secondary mirror, 5 - 14 μm circular variable filter (CVF) and fixed filter wheels, and the array at the de-magnified image of the focal plane. The cold optics are contained in a baffle system within the LHe temperature radiation shield to minimize light leaks.

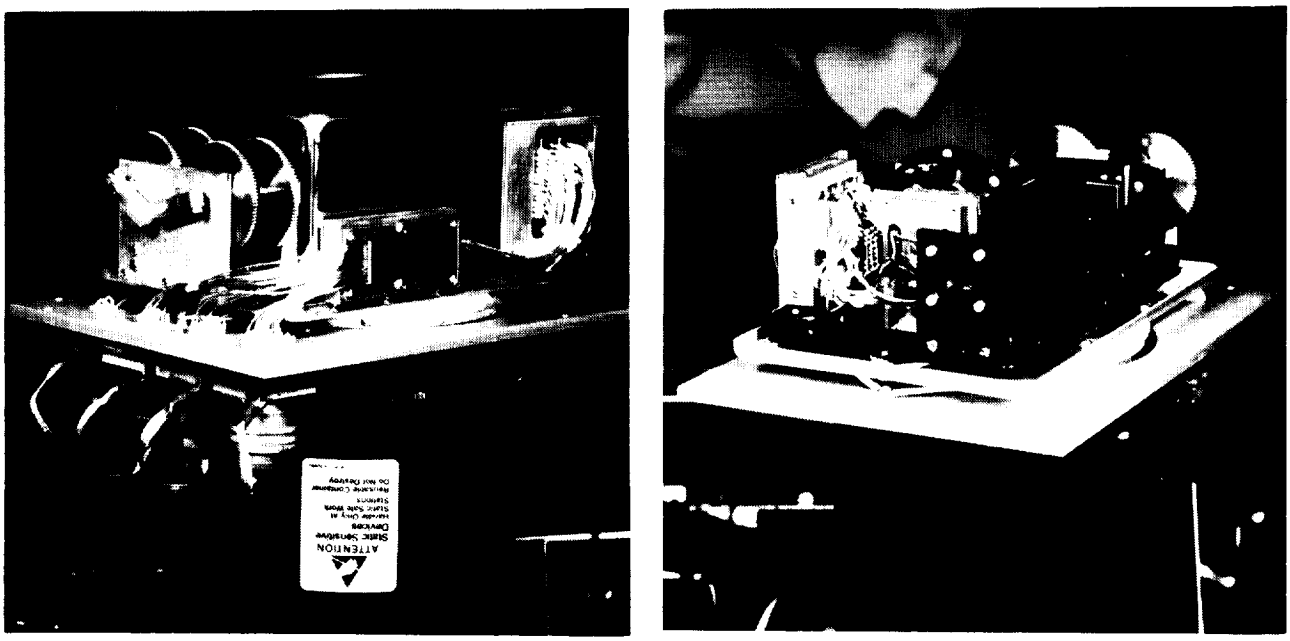

Figure 3: Two views of the cryogenic optical bench assembly with the dewar inverted and vacuum housing and LN_2 shield removed. Left: The LHe temperature cold shield housing, individual stainless steel micro-coax wiring feeding through a heat-sink maze at the LN_2 shield, the LN_2 temperature bulkhead and drive gears for the two filter wheel shafts, connector bulkhead at the LHe shield, and connectors on the warm vacuum housing cover. Right: View from the opposite side with LHe housing removed, showing the square off-axis parabolic mirror segment (right) in front of the filter drive gears, the fixed and circular variable filter wheels (center) behind the cold array mounting block, and the micro-coax cold connector bulkhead (left).

on the IRTF. Aberrations are negligible and field rotation and distortion (pin cushion, etc.) across the array are less than 1/2 pixel across the full field of the detector (<0.5 degrees). The cryogenic optical assembly is shown in Figure 3.

Sensitivity and Noise Performance:

On the telescope the detector is background-limited; electronic system noise, detector read noise and dark current noise are negligible (<200 electrons) compared to total background and sky noise of roughly 1000 electrons (depending on telescope temperature and weather conditions) per 30 msec integration. The array camera NEFD (noise equivalent flux density) at 10 μm on the IRTF is NEFD = 0.05 Jy pixel^{-1}min$^{-1/2}$ (1σ) for extended sources, a source surface brightness of 0.7 Jy arcsec^{-2}. The NEFD for point sources is about 0.7 Jy min$^{-1/2}$ since the diffraction/seeing limit is typically about 1 arcsec and the point source flux is spread among a number of pixels. (*Note added in proof:* The effective well capacity was recently trippled by reducing the net bias to 4 volts, thus reducing G_{pc}, to permit the use of 10% bandwidth interference filters. This resulted in a S/N improvement of about 2 due primarily to improved photon statistics).

ASTRONOMICAL RESULTS:

The Galactic Center - Arcsecond Scale Structure and Dust/Gas Ratio:

Seeing-limited images of the central 16 arcsec (0.8 parsec) field of the Galactic Center obtained at 7.8, 9.8, 11.6 (Figure 4a) and 12.4 μm with the DRO array camera reveal new structural details in the infrared dust distribution on the 1 arcsec scale. In addition, a mosiac image with the same resolution of the 50 x 90 arcsec field in the vicinity of the Sgr A West complex has been developed from 20 individual 1 min integrations at 12.4 μm (Figure 4b). These results are discussed in detail by Gezari (1989b).

The new array results show structure which is strikingly similar to the ionized gas emission features seen in VLA maps (Yusef-Zadeh 1988), and in the Br α and Br γ near infrared array images (Forrest et al. 1986). However, the warm dust and ionized gas distributions show significant discrepancies in the positions of several of the bright peaks (Gezari 1988b).

A detailed comparison of the 11.6 μm array image (Figures 4a, 5a) and 6-cm continuum VLA image (Figure 5b) with the same (1 arcsec) spatial resolution has been made (Yusef-Zadeh and Gezari 1989). The most pronounced positional shift is seen at the positions of IRS 2 and nearby IRS 13. These two sources lie at the western edge of a 2 arcsec mini-cavity which was recently noted in the sub-arcsecond resolution VLA map of Sgr A West (Yusef-Zadeh et al. 1988). The relative infrared and radio emission intensities may be due to stellar wind which has produced the mini-cavity and which has depleted the dust paricles at the inner edge of the cavity close to the source of outflow.

Figure 5(c) shows the dust-to-gas ratio calculated from the two data sets. Differences between the warm dust and ionized gas distributions along the major source structures in the complex are evident as varaitions in the 11.6-μm/2-cm dust-to-gas ratio calculated from the two data sets. Considering the high relative positional accuracy ($\pm$ 0.1 arcsec) and comparable spatial resolution (1 arcsec), the relative source positions and derived dust-to-gas ratio are significant. The spatial variation of R may be due to a

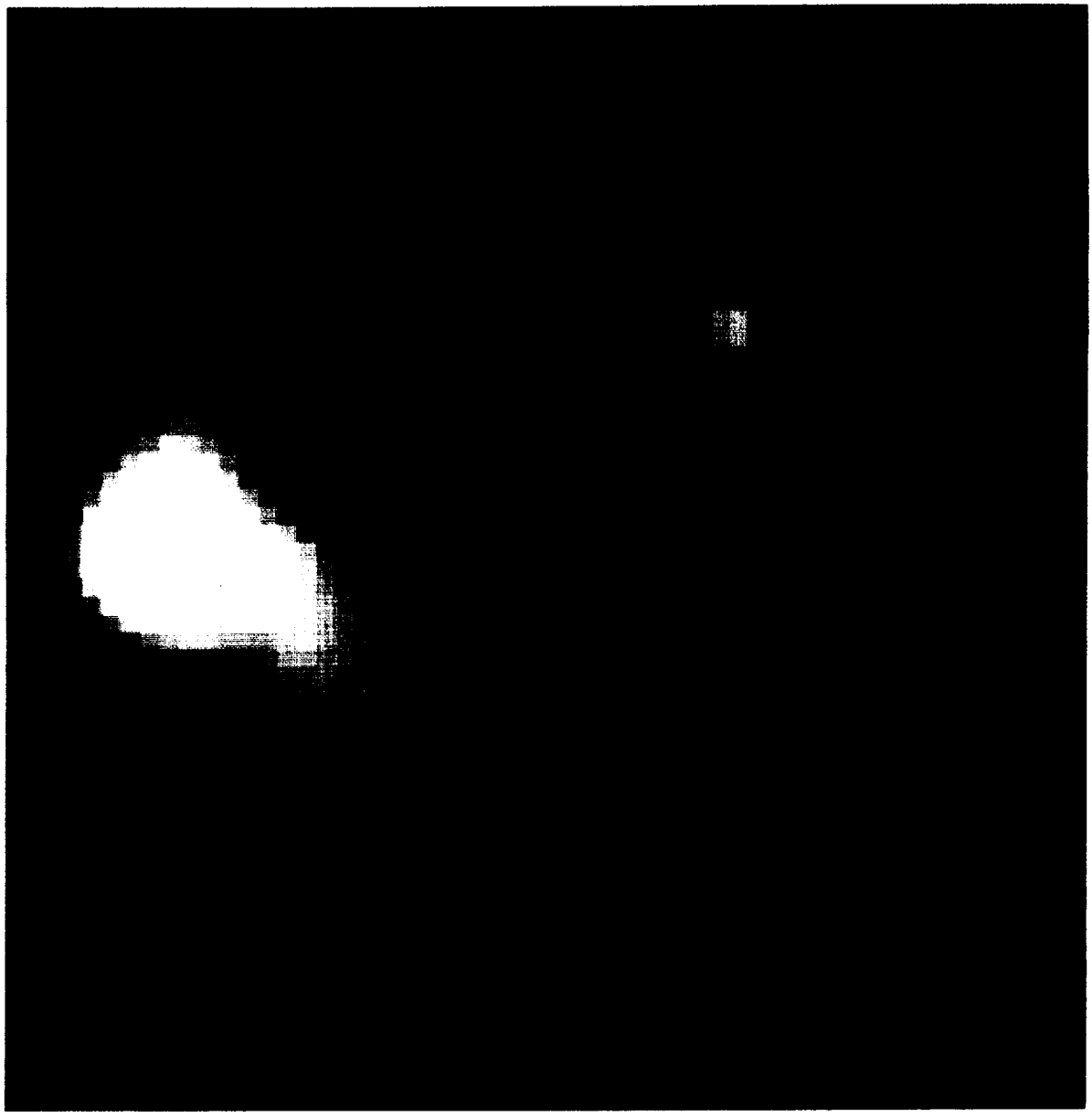

Figure 4a: 11.6 μm array camera image of the central 0.8 parsec (16 arcsec) of the galactic center, coadded from four individual 1 min long integrations on the 3-m IRTF Telescope. This 1 arcsec resolution image shows the curved ridge and bright compact sources surrounding the non-thermal point source Sgr A* (not detected, at the center of the image) and reveals extended infrared source structure similar to the Brackett α and 6-cm continuum VLA distributions, with notable discrepancies in the positions of several bright peaks. The results are discussed in detail by Gezari (1989b).

Figure 4b: A preliminary 12.4 μm mosiac image of the Sgr A West complex assembled from 20 individual 1 min integrations, covering an area of about 50 x 90 arcsec (top 20 arcsec not shown). The brightness scale is logarithmic, from about 1 - 20 Jy arcsec^{-2}. The central field shown in Figure 4a is seen in this large scale image as the saturated ridge at lower-center (approximately 2-inches square). Details in Gezari (1989b).

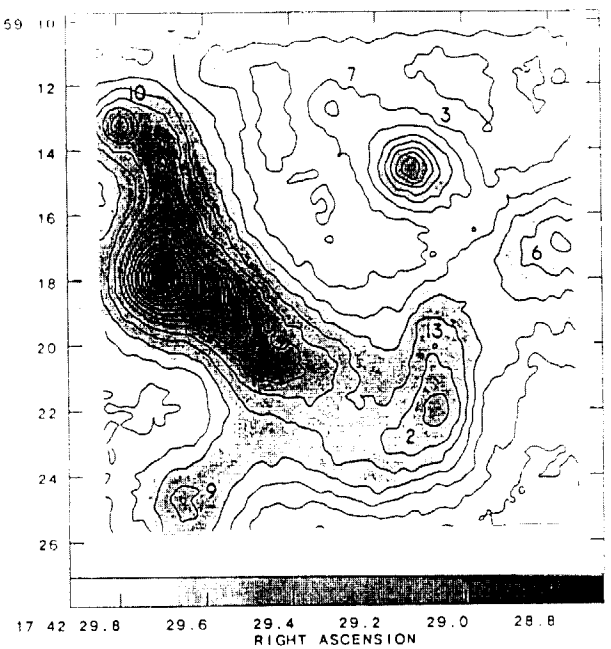

Figure 5(a): Calibrated contour map of 11.6 μm flux density from the central 1 pc of the Galactic Center, corresponding to the seeing-limited (1 arcsec) array image in Figure 4. The contour interval is 1 Jy arcsec^{-2} to the peak brightness of 16 Jy arcsec^{-2} at IRS 1.

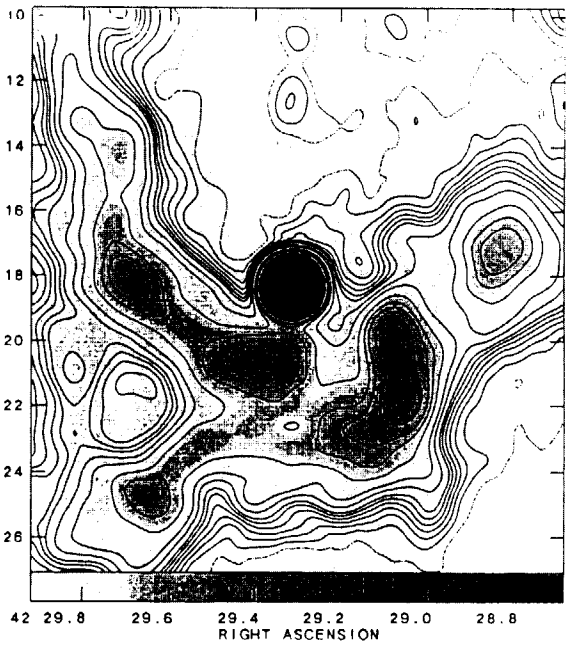

Figure 5(b): VLA map of calibrated 6-cm brightness in the Galactic Center displayed in quasi-logamithmic contours (from about 0 to 200 mJy/ beam) with the saturated peak = 1.2 Jy/beam at Sgr A*.

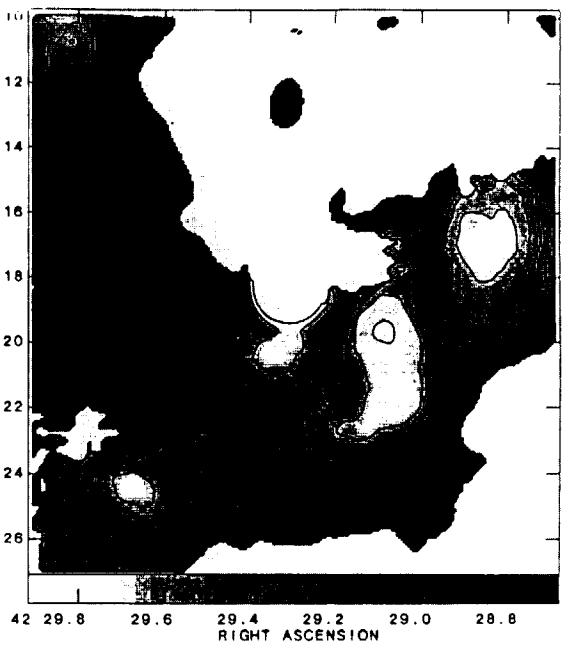

Figure 5(c): The dust-to-gas ratio calculated from the data sets in Figures 5(a) and 5(b). The dust-to-gas brightness ratio ranges from about 50 near IRS 13 to ~275 about 2 arcsec west of IRS 10. Darker grey regions richer in dust, lighter grey regions are relatively dust depleated. The ratio in areas away from the ridge and strong sources is reliable in the black regions ($300 < R < 700$).

non-constant value of dust to gas ratio, or, it may suggest that sources of heating other than a central source at IRS16/Sgr A* may be embedded along the ionized filaments in Sgr A West and contribute to the heating of the intermixed dust. Regarding the question of the luminosity source of the Sgr A West complex, the results suggest that a combination of a central external ionizing luminosity source near Sgr A*/IRS16 and internal heating by imbedded sources with somewhat softer spectra at several of the bright peaks is responsible for the observed infrared and radio contimuum emission. These results are presented in detail by Yusef-Zadeh and Gezari (1989).

5 μm Speckle Interferometry of IRC +10216:

The array camera has been used to make two-dimensional 5 micron speckle interferometry observations of IRC+10216, which resolve sub-arcsec source structure in the presence of seeing and telescope aberations. Fifty separate 5 μm short exposure (1/30 sec) narrow band $\Delta\lambda/\lambda = 0.02$) images of IRC+10216 were taken (Figure 6a) as well as fifty images of reference star R Leo obtained under the same conditions (Figure 6b). The individual exposures in each set were separated by about 15 seconds.

The data were obtained at the Mauna Kea 3-m IRTF telescope in March 1988. Pixel size = 0.26 arcsec square, and the diffraction limit of the 3-meter IRTF telescope is $\theta = 0.35$ arcsec (FWHM) at 5 μm, thus the diffraction-limited speckle image detail was not fully sampled. Seeing was excellent (estimated at about 1/2 arcsec). Therefore only the central few speckles in each image were illuminated and differences between the images appear primarily as seeing-induced image wobble.

The two sets of speckle images images were processed (Gezari, Nisenson and Stachnik 1989) using four techniques: 1) centered direct sums (shift-and-add) of the images, 2) two-dimensional speckle interferometry (power spectrum analysis), 3) iterative deconvolution of one data set by the other, and 4) Knox-Thompson speckle imaging processing. R Leo was used as a reference star because of its proximity to IRC+10216 and comparable brightness at 5μm (ratio about 3:4), minimizing instrumental effects. The spatial structure results obtained by all methods are generally consistent with a slightly asymmetric resolved source of average diameter ~0.65 arcsec (FWHM). The Knox-Thompson speckle imaging reconstruction, the iterative convolution of IRC+10216 by R Leo, and the ratio of their power spectra all show a spatial asymmetry in IRC+10216.

The corrected diameter of IRC+10216 vs. position angle on the sky (north = 0^o) derived from fits of an Airy function to cuts through the ratio of the power spectra at 10^o intervals. A maximum asymmetry of about 20% is evident at a position angle of about 25^o with maximum diameter of about 0.75 arcsec. The apparent 5 μm source assymetry detected here is consistent with the 4.6 μm measurements of Mariotti et al. (1983), but not as large as the effects reported by McCarthy, Howell and Low (1980), Dyck et al. (1984), and Ridgeway and Keady (1988). As these authors point out, the observed infrared fringe visibility of IRC+10216 is complex, wavelength and possibly time dependent, and more extensive two-dimensional speckle observations on a larger telescope are planned. This work is presented in detail by Gezari, Nisenson and Stachnik (1989).

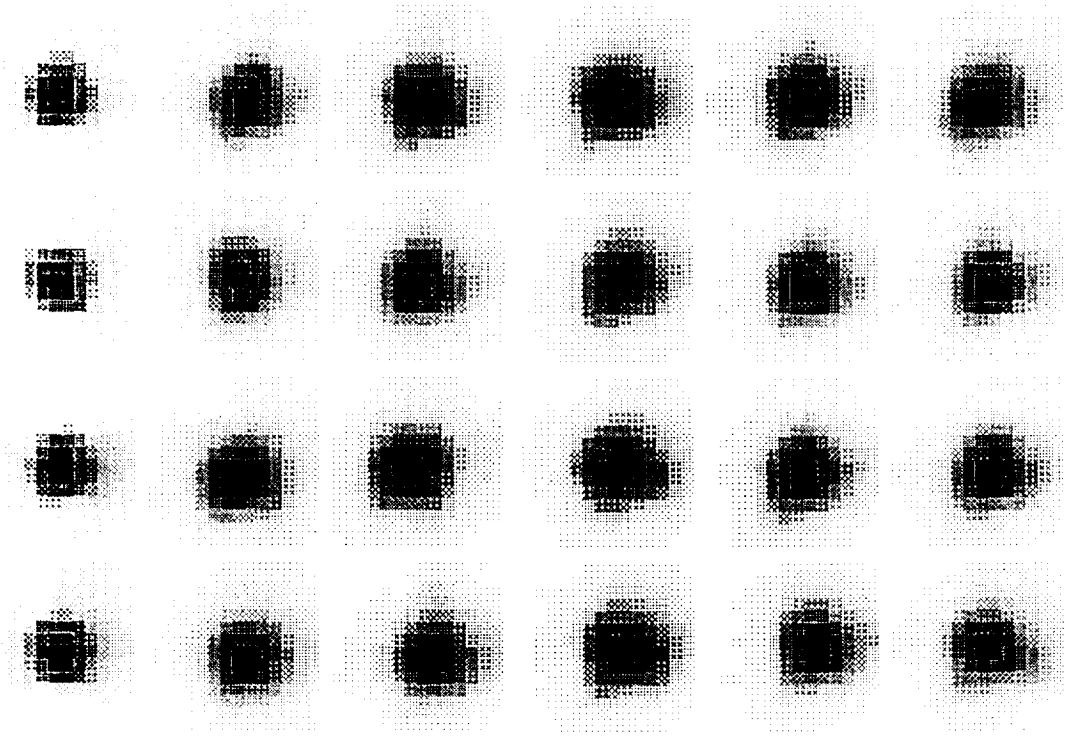

Figure 6(a): Individual short exposure (1/30 sec) narrow band ($\Delta\lambda/\lambda = 0.02$) speckle interferometry observations of IRC+10216 taken at 5 μm in March 1988 (Gezari et al. 1988). The pixel size = 0.26 arcsec, and the diffraction limit of the 3-meter IRTF telescope is $\theta = 0.35$ arcsec at 5 μm. Seeing was excellent (estimated at <1/2 arcsec).

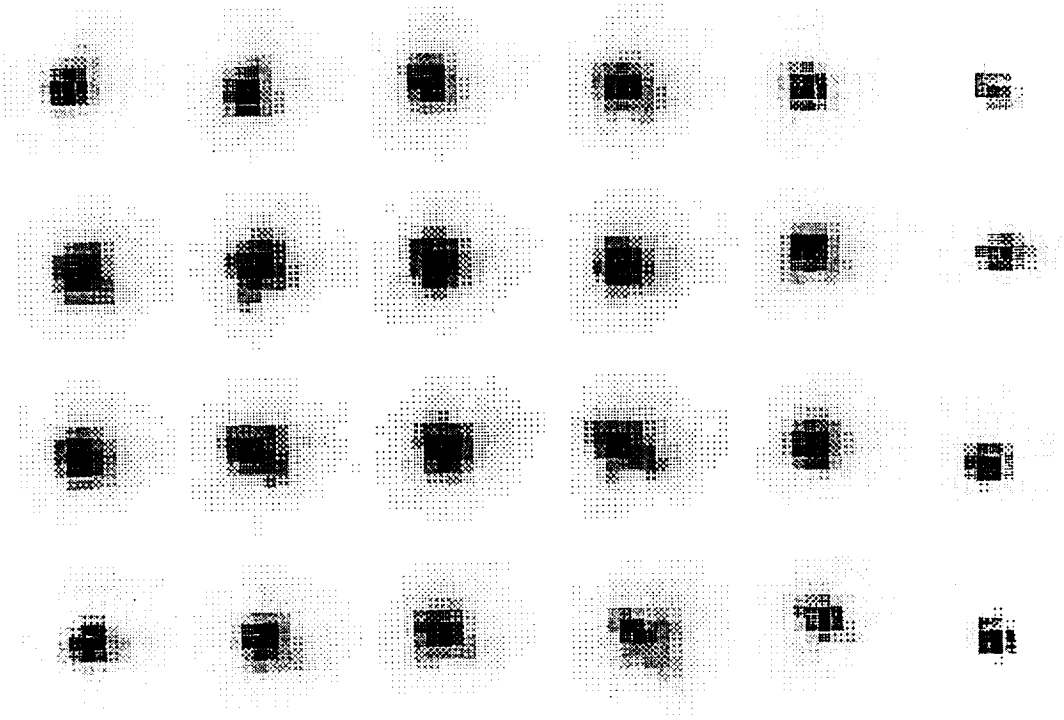

Figure 6(b): Reference star R Leo, obtained under the same conditions as in 6(a). R Leo and IRC+10216 are at the same airmass and are of of comparable brightness at 5μm. The two sets of images are displayed normalized to the peak brightness in each image.

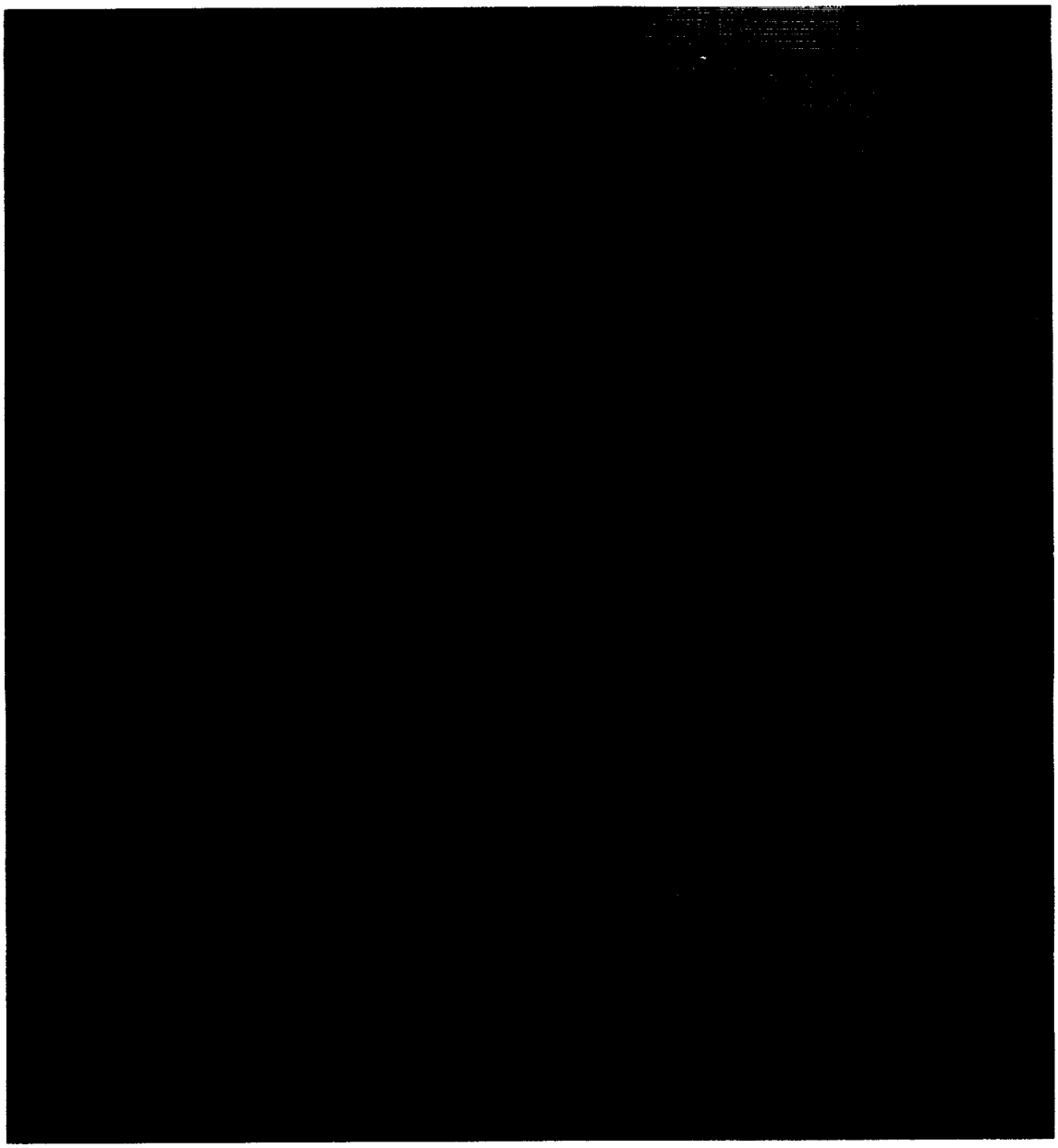

Figure 10: 12.4 μm array camera image of Orion BN/KL. BN is at top, IRc4 (KL) is at bottom, IRc7 is at center, IRc2 is left of center, and the IRc2 ridge source, identified with the SiO maser and the H_2O maser cluster, connects them. The array pixels are 0.26 arcsec and the image size on the 3-m IRTF was 1.0 arcsec (FWHM).

New 12.4 μm Source Structure in Orion BN/KL "IRc2":

Orion "IRc2" was proposed to be the primary luminosity source in the detailed model for the energetics of the Orion BN/KL infrared nebula (Wynn-Williams et al. 1984) based on 2 arcsec aperture photometry. Seeing-limited array imaging at 12.4 μm has resolved complex 1 arcsec scale structure in "IRc2", showing two equally bright compact objects connected by a narrow ridge of emission (Figures 10, 12, 14). One of these is IRc7 (previously thought of only as a significant source at 20 μm) and the other is the true IRc2 (3.2 arcsec to the east). A new, partially resolved ridge source extends from IRc2 toward IRc7. The Orion SiO maser is located at the end of the ridge and the surrounding elongated cluster of H_2O masers is aligned along the ridge, to within the present radio and infrared array positional errors. The small-scale structure of IRc2 ridge source can not be attributed to the effects of "bad pixels" or other array gain defects. Considering the high intrinsic accuracy of the relative array astrometry presented here, the detailed structure of the 12 μm sources and the coincidence of the IRc2 ridge with the SiO/H_2O maser cluster are significant. The SiO maser does not coincide with IRc2, but with the ridge source; thus the SiO maser is not directly identifiable with a high luminosity infrared source. Conversely, it appears that IRc7 is more luminous than previously thought.

Three other new infrared objects have been detected in the complex. One of these is an 8.7 point source 2 arcsec south of IRc7 at the position of the 3.8 μm object "n" (see Figure 11). Careful inspection shows evidence of this object in the 12.4 μm map as well. Two additional new compact 12.4 μm sources are found about 3 arcsec east of IRc2 (see Figure 12). These three new sources are somewhat fainter than IRc3 and IRc6, but are unambiguously detected. The image of IRc4 (KL) is elongated in the N-S direction and resolves considerably more structure than previous results. IRc4 is comparable in peak brightness to but somewhat more extended than IRc2 and IRc7.

There are other indications that the luminosity of the region is not attributable to a single powerful object. The center of outflow low-velocity masers (Genzel et al. 1981) is midway between IRc7 and IRc4 (KL), a significant displacement from the compact IRc2 array source on the scale of the present astrometry. Further, inspection of the 3.8 μm polarization observations by Werner, Dinerstein and Capps (1983) suggests that the vectors point back to at least three equally likely positions near BN, IRc7, and a point east of IRc2. The new array results as well as these factors suggest that a number of sources contribute to the total luminosity of the region, including IRc7, IRc2, IRc4 (KL), several new objects, and BN itself. Complete details of the photometry and astrometry of the BN/KL IRc2 complex, including exact placement of the maser cluster (to within the $\pm$ 0.1 arcsec achievable error), will be presented by Gezari (1989a).

OBSERVATIONAL CONSIDERATIONS:

Calibration:

The reduction of 10μm astronomical array data involves a particuliar set of concerns which arise from observing in a high background, low signal-to-background regime. Drifts in the array gain matrix and the thermal background from the sky or telescope on time scales comparable to the integration or calibration intervals can result in increased noise and image defects. The remedy in many cases is real-time chopping with the telescope secondary mirror. In general, several kinds of array image data must be obtained to produce a final calibrated image set at each wavelength. These include: source data frames, blank sky

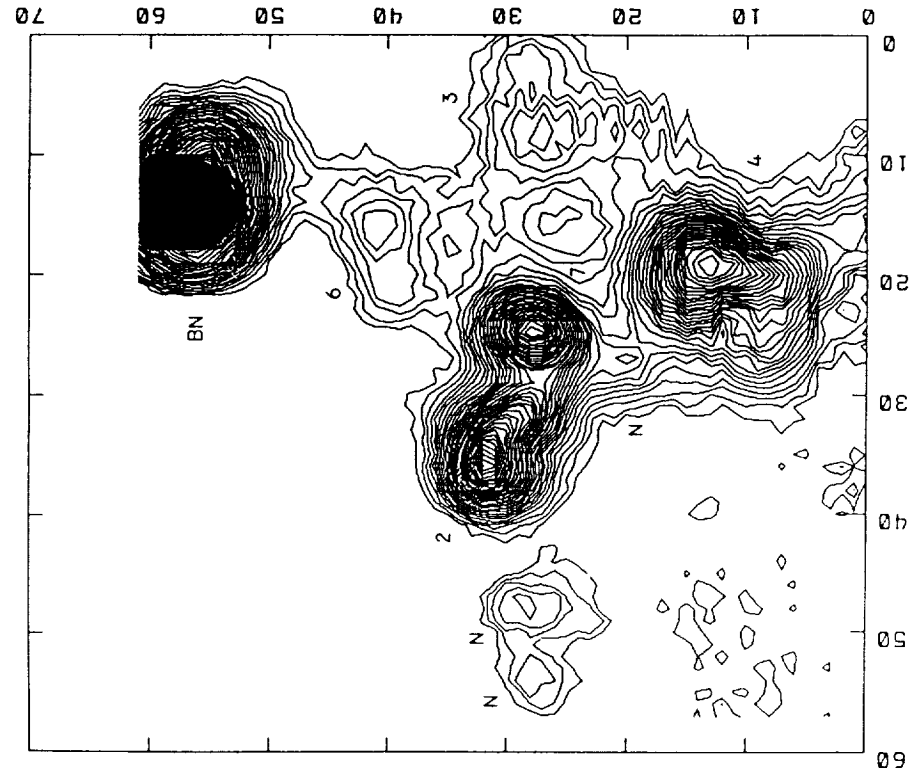

Figure 12: Contour plot of Orion BN/KL at 12.4 μm. The IRc source numbers are indicated. New sources are seen to the east of IRc2, and there is evidence of the new 8.7 source south of IRc7. Structure in the ridge extending from IRc2 toward IRc7 is slightly smoothed as result of mosiacing four shifted 1 min integration images. The axes are labled in pixel numbers.

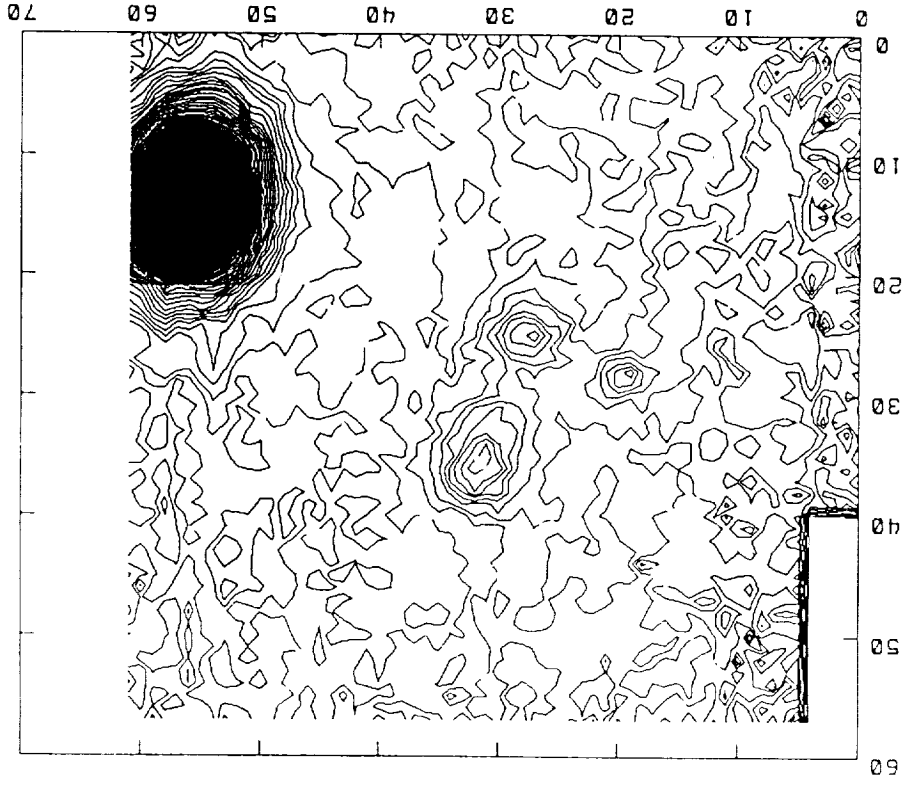

Figure 11: Contour plot of Orion BN/KL at 8.7 μm. The new 8.7 μm source is 2 arcsec south and slightly east of IRc7.

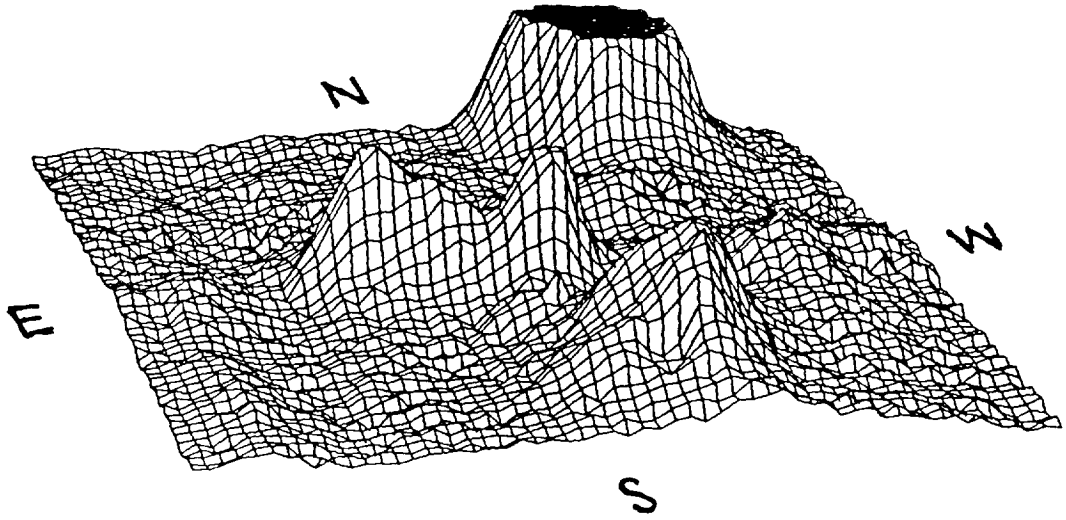

Figure 13: Plot of 12.4 μm Orion BN/KL intensity in one array field as viewed from the "southeast". BN is truncated at the top, IRc7 is the sharp peak south of it, IRc2 is to the east, and the ridge extending from IRc2 toward IRc7 is associated with the cloud of SiO and H_2O masers. IRc4 (KL) at the south, and IRc6 and IRc3 are evident north and west of it.

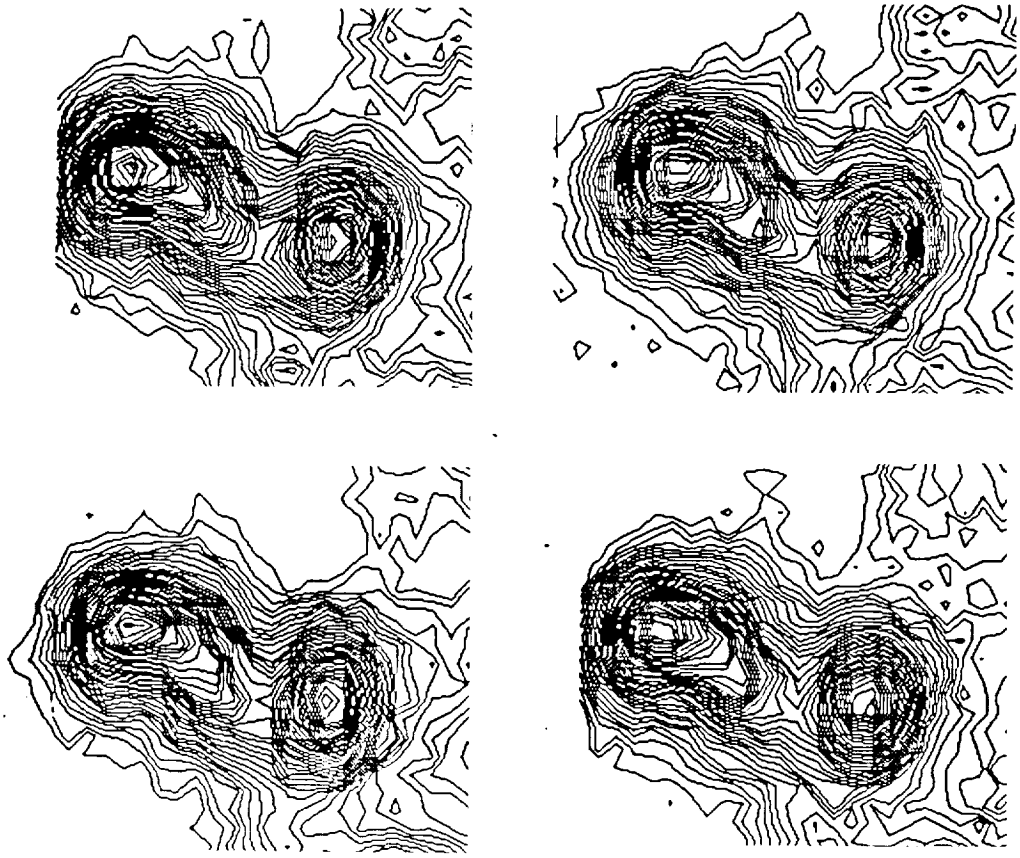

Figure 14: Four individual 1-min integrations of IRc2-IRc7 taken on different parts of the array to illustrate the flat-field uniformity and reproducibility of the array data. These unsmoothed images suggest some additional detail in the IRc2 ridge source.

frame(s) for sky/telescope backround subtraction and removal of residual spatial offsets, additional sky frames at high and low airmasses for flat-fielding, standard star frames for flux calibration and atmospheric extinction correction, and a (cold shutter) dark frame for some detector sampling schemes. The calibration images must have the same noise characteristics (usually equal integration time) as each of the individual data images to be corrected. In single sampling, images used individually are also corrected by subtracting a dark (cold shutter) frame.

Flat-Fielding:

Flat-fielding (gain matrix correction) of a source images requires the image of a a uniform field (usually blank sky) as a map of the net instrumental gain effects due to two-dimensional array, system, and telescope offsets. The basic approach to flat-fielding high-background array image data (after sky subtraction) is to divide the sky subtracted image by a normalized blank sky frame. The blank field image used for the division can be the sky image obtained while chopping, or another sky frame obtained under the same system gain and sky background conditions. A gain matrix constructed by subtracting high and low airmass sky images provides a more rigorous flat field correction. In practice, one or the other of these approaches will occasionally and inexplicably fail, resulting in defects in the image. Under good conditions *in principle* the same flat-field frame could be used for many different data images. However, the temperatures of the sky, telescope and detector, the sky opacity, and the gain of the electronic system must be stable on the time scale of the individual observations. In practice, flat fielding is most successful using nearly symultaneous chopped sky data. Flat-fielding of high-background array data can be the single most demanding calibration requirement.

Plate Scale Calibration:

To take full advantage of the potential intrinsic astrometric precision of the array, the plate scale of the array on the telescope (including linear scale in both dimensions, rotation, and distortion) must be accurately calibrated. This seemingly straightforward task is frustrated by a lack of two or more visual position standard stars in a single array field of view which are also easily detected at 10 μm. Measurements of a star moved around the array (once confidence in the telescope position encoders has been established), combined with lab tests using grid targets, are the basic calibration methods. Considerable effort was put into obtaining an accurate array plate scale, and one should be forewarded that an array camera optical system with variable magnification (zoom) capability (Gezari 1988a) could present a plate scale calibration burden which might outweigh any advantage of flexibility.

Is Chopping Necessary with 10 μm Array Detectors?

In principle chopping is not required for sky background subtraction or flat-fielding of high-background array image data. The ability to make infrared array observations without a chopping secondary would provide significant practical advantages. No telescope chopper mechanism would be needed (a real concern in the design of large next-generation telescopes), and improvement in observational duty cycle of more than a factor of 2 could be achieved over continuous chopping (since the array is on the source only half the time, data is not taken while the chopper switches position and stabilizes). Image quality and astrometric accuracy can become limited by chopper positional stability errors, rather than by optical aberration, focus, or atmospheric seeing, although we have not seen this problem on the IRTF except when attempting chopper rates slower than 1 Hz.

Sky subtraction could be done without chopping if a single pixel in the source image was known to contain blank sky *and* an accurate gain matrix existed for the array system for those observing conditions. The two could be used to create a synthetic sky frame for background subtraction. Sky and offset subtraction can also done by shifting the position of the source on the array, subtracting shifted frames, and deconvolving the source data. System gain stability is critical in these schemes. In practice, sky subtraction using these alternate methods is not routinely accomplished, but it is actively being pursued. Because of the sensitivity of the photon image and system gain matrix to environmental factors, slow (1 Hz) chopping against blank sky remains the least risky approach since it provides real-time sky subtraction and gain matrix data at what is a reasonable cost in observing time. Eventually, with additional experience and system improvements, chopping will probably not be necessary for high-background array observations.

Putting the Array Camera Performance in Perspective:

The signal-to-noise performance of the photoconductor array camera on the IRTF at 10-μm can be compared to the IRTF broad-band single germanium bolometer system (2 arcsec circular aperture, $\Delta\lambda$ = 5μm, and η = 1, NEFD ~ 23 mJy min$^{-1/2}$) by scaling instrumental parameters. If the array pixels were binned up to equal the bolometer aperture, the single bolometer would have a S/N advantage of a factor of about 5 over the synthetic binned photoconductor array "pixel", which is accounted for by the differing $\eta^{-1/2}$ and $\Delta\lambda^{-1/2}$ factors. Scaled to the parameters of the IRTF bolometer, the observationally measured array NEFD would be about 40 mJy min^{-1}pixel^{-1}, compared to the claimed 23 mJy min^{-1}pixel^{-1} for the bolometer. This factor of 2 discrepancy can be accounted for in part by uncertainty in scaling parameters and the likelihood that the IRTF bolometer noise performance is somewhat worse than the 3 mJy hr$^{-1/2}$ claimed.

Arrays have significant advantages over single detectors for high resolution mapping of extended sources. In general, the main advantage of arrays is their increased detector area per unit integration time. Symultaneous photometry and astrometry over 3596 points on the sky, with small pixels to sample diffraction-limited information, and bandwidth narrow enough to do photometry in the standard infrared bands is extremely attractive. But arrays present no advantage in observing compact sources (where most of the array is not utilized) except for problems involving small scale structure or a search for new objects.

The array performance numbers can be somewhat misleading. Consider that a 5σ detection takes 25 times longer than the stated 1σ NEFD figure, that NEFD per pixel numbers can seem deceptively low simply because array pixels are small, that diffraction and seeing spread the flux from a point source over at least 10 pixels and, and that chopping more than doubles the elapsed time. Calibration sources and flat fields generally have to be observed to the same noise level as the in the source image data, and multi-color observations further multiply the total observing time. It is relatively "easy" to image a cluster of ~30 Jy sources like Sgr A West in a 1 minute integration with high signal/noise. A cluster of 1 Jy sources could be detected in 1 minute, but getting an image of them with signal-to-noise comparable to the Sgr A West image would take 1,000 times longer, a sobering prospect. However, it is also true that an array can make mapping observations which would be completely impractical to attempt with a single detector. Each device should therefore be applied to the observations for which it is best suited.

ACKNOWLEDGMENTS

We are grateful to Mary Hewitt for her expert guidance on behalf of Hughes/Santa Barbara Research Center, and to Alan Hoffman, Geof Orias and Carol Oania of SBRC for their valuable advice and support of the DRO Camera program. We acknowledge stimulating discussions with Dick Joyce, Bill Hoffmann, Ian Gatley, Nick Scoville, Chas Beichman, Mark McCaughrean, Reinhart Genzel and Eric Becklin. We thank Gordon Chin for advice on the A/D converter concept and opto-isolation techniques, and Katherine E. (Katie) Boone for her skillful system software support. This research is funded by NASA RTOP 188-41-55 and the Goddard Director's Discretionary Fund.

BIBLIOGRAPHY

Deming, L. D., Mumma, M., Espenak, F., and Gezari, D. 1989 (in preparation).
Dyck, H. M., Zuckerman, B., Leinert, C. and Beckwith, S. 1984, Ap. J., 287, 801.
Folz, W. 1988, NASA Technical Memorandum, #TM-(in press).
Fowler, A., Probst, R., Britt, J., Joyce, R., Gillett, F. 1987a, Opt. Engr., 26, 232.
Fowler, A., Gillett, F., Gregory, B., Joyce, R., Probst, R., Smith, R. 1987b, Infrared Astronomy With Arrays (Proc. Hilo Detector Workshop, Univ. of Hawaii), 197.
Forrest, W. J., Shure, M. A., Pipher, J. L. and Woodward, C. E. 1986, Proc. Townes Symposium on the Galactic Center, (American Institute of Physics, 155), 127.
Gezari, D. Y. 1988a, NASA Technical Memorandum, # TM-(in press).
Gezari, D. Y. 1988b, Proc. IAU Symposium #136 Galactic Center (UCLA), in press.
Gezari, D. Y. 1989, (in preparation for Ap. J. (Letters)).
Gezari, D. Y. 1989b, (in preparation for Ap.J.).
Gezari, D. Y., Folz, W. C., Woods, L. A., Wooldridge, J. 1988, Proc. S.P.I.E., 973.
Gezari, D. Y., Mumma, M., Espenak, F. and Demming, D. 1989, (submitted to Nature (Letters).
Gezari, D. Y., Nisenson, P. and Stachnik, R. V. 1989, B. A. A. S. (Abstract), Boston 1/89, (in preparation for Ap. J. (Letters))
Hoffman, A. W. 1987, Infrared Astronomy With Arrays (Proc. Hilo Detector Workshop 5/88), Univ. of Hawaii, 29.
McCaughrean, M. J. 1988, Ph.D. Thesis, University of Edinburgh.
McKelvey, M. E., Goebel, J. H., McCreight, C. R., Moss, N. N. 1987, Infrared Astronomy With Arrays (Proc. Hilo Detector Workshop 5/88), Univ. of Hawaii, 140.
McLean, I., Chuter, T., McCaughrean, M., Rayner, J. 1986, Proc. S.P.I.E., 627, 430.
Ninkov, Z., Forrest, W. J., Pipher, J. L. 1987, Infrared Astronomy With Arrays (Proc. Hilo Detector Workshop 5/88), Univ. of Hawaii, 37.
Mariotti, J., Chelli, A., Foy, R., Lena, P., Sebille, F., and Tchountonov, G. 1983, Astron. Astrophys., 120, 237.
McCarthy, D., Howell R. and Low, F. 1980, Ap. J. (Letters), 235, L27.
Ridgeway S. and Keady J. 1988, Ap. J., 326, 843.
Werner, M. W., Dinerstein, H. L., and Capps, R. W. 1983, Ap. J. Letters, 265, L13.
Wynn-Williams, C. G., Genzel, R., Becklin, E. E., and Downes, D. 1984, Ap. J., 281, 172.
Yusef-Zadeh, F. 1988, private communication.
Yusef-Zadeh, F. and Gezari, D. Y. 1989, B. A. A. S. (Abstract), Boston 1/89 (in preparation for Ap. J. (Letters)).
Yusef-Zadeh, F., Morris, M., and Eckers, R. 1988, Proc. IAU Symposium #136: Galactic Center, (UCLA 8/88), in press.